CrystEngComm

Dynamic Article Links

Cite this: *CrystEngComm*, 2012, **14**, 1783

www.rsc.org/crystengcomm

PAPER

Ammonium sulfate regulation of morphology of Nd:Y_2O_3 precursor *via* urea precipitation method and its effect on the sintering properties of Nd:Y_2O_3 nanopowders

Haiming Qin,[a] Hong Liu,*[a] Yuanhua Sang,[a] Yaohui Lv,[b] Xiaolin Zhang,[a] Yuanyuan Zhang,[a] Tadashi Ohachi[c] and Jiyang Wang*[a]

Received 19th September 2011, Accepted 12th November 2011
DOI: 10.1039/c1ce06230a

Ammonium sulfate has been widely used as a control agent in the preparation of yttrium-aluminium-garnet (YAG) transparent ceramics, however, research of its application in the preparation in transparent ceramic yttria has not been intensively studied. Neodymium–doped yttria (Nd:Y_2O_3) nanopowders with controlled morphology and size were synthesized *via* a urea precipitation method using ammonium sulfate as the additive. The effect of ammonium sulfate was intensively studied throughout the preparation process. Morphology of precursors was found to be evidently affected by the [$(NH_4)_2SO_4$]/[Nd:Y_2O_3] ratio (measured by weight). Uniform spheres of Nd:Y_2O_3 precursor were obtained without the addition of ammonium sulfate. With increasing amounts of ammonium sulfate added, the scale of the Nd:Y_2O_3 precursors diminished which results in the aggregation of the Nd:Y_2O_3 precursor. Aggregates of coral like particles after precipitation and uniform well dispersed particles after calcinations were obtained as the dosage of ammonium sulfate reached 20 wt%. It was considered to be the optimum state for the preparation of highly sinterable Nd:Y_2O_3 nanopowders. Ammonium sulfate was proved to be a regulator that could mediate the nucleation and growth of the precursor as well as its decomposition behaviour. Results of this paper can contribute to the controllable synthesis of transparent ceramic yttria.

Introduction

Yttria materials are attractive for use in laser mediums and luminescent materials mainly because of their excellent chemical and physical properties.[1–3] The cubic Y_2O_3 single crystal has several favorable properties such as its refractory nature, physical and chemical stability, and optical clarity over a broad spectral range from 280 nm to 8 μm.[4–9] The thermal conductivity of undoped Y_2O_3 (27 W m^{-1} K^{-1}) was reported to be nearly twice as large as that of YAG (11 W m^{-1} K^{-1}) according to Klein and Croft's report.[10] All those advantages make yttria one of the most promising candidates as a host material for laser media. However, a high melting point up to 2430 °C and the phase change from cubic to hexagonal structure at 2325 °C causes extreme difficulty for the growth of cubic type yttria single crystals using the melt growth method, while the flux growth of Y_2O_3 would inevitably introduce impurities into the crystalline sturucture.[11,12] With the development of techniques for preparation of transparent ceramics, transparent Y_2O_3 ceramics became the substitute for single crystals. After the first fabrication of transparent Nd:Y_2O_3 ceramics by Anderson in 1972,[4] Yanagitani reported a vacuum sintering method to fabricate highly transparent YAG ceramic laser materials where raw materials were prepared by nanotechnology in 1999.[13,14] However, the controllable preparation of transparent ceramic yttria from nanopowders remains a huge challenge. Extremely high sintering temperatures, up to 2000 °C under vacuum or 1850 °C in hydrogen atmosphere, are required to prepare highly transparent lanthanide doped yttria ceramics.[15,16] The other technology is hot pressing or hot isostatic pressing, in which high pressure is applied during the sintering stage.[16] Although the hot pressing or hot isotatic pressing is usually effective for obtaining high quality transparent ceramics, the use of high-pressure equipment results in high running costs and risk. Further studies on the preparation process, especially the precipitation of the precursor, to obtain highly sinterable yttria nanopowders is quite necessary. Synthesis of high quality nanopowders is the first and key step for preparation of highly transparent yttria ceramics. Many efforts were paid for obtaining high quality yttria nano particles through different synthesis methods, such as decomposition of yttrium salts,[17] precipitation methods,[2,3,18–25]

[a]*State Key Laboratory of Crystal Materials, Shandong University, Jinan, 250100, China. E-mail: hongliu@sdu.edu.cn; Jywang@sdu.edu.cn; Fax: +86-531-88362807; Tel: +86-531-88362807*
[b]*School of Materials Science and Engineering, Anhui University of Technology, Maanshan, 241002, China*
[c]*Department of Electrical Engineering, Doshisha University, Kyotanabe, Kyoto, 610-0321, Japan*

This journal is © The Royal Society of Chemistry 2012

hydrothermal synthesis,[26–29] emulsion synthesis,[30] spray–drying,[31,32] sol–gel synthesis,[33–37] and combustion synthesis,[38,39] *etc*. Among which, precipitation methods are attractive because of their accessibility. Monodispersed spherical nanosized yttria precursors were prepared *via* a urea precipitation method.[2,3,23,25] Most developed methods for synthesis of sinterable yttria powders always involve the addition of ammonium sulfate.[21,22,43] However, the function of ammonium sulfate has not yet been discussed. In this paper, the effect of ammonium sulfate was intensively studied throughout the preparation process. Special attention was paid to the mechanism of the precipitation process and the effect of ammonium sulfate was intensively studied throughout the preparation process. It was found that the morphology, microstructure and sinterability of the calcined powders were highly affected by the $[(NH_4)_2SO_4]/[Nd:Y_2O_3]$ ratio. Ammonium sulfate was proved to be a regulator that could mediate the nucleation and growth of the precursor. Results shown in this paper can contribute to the controllable synthesis of sinterable yttria nanopowders and further exploration of the mechanism of the precipitation process *via* the urea precipitation method.

Experimental

In a typical synthetic procedure for colloidal precursor particles, proper amounts of $Y(NO_3)_3 \cdot 6H_2O$ (Alfa Aesar, 99.99%), $Nd(NO_3)_3 \cdot 6H_2O$ and urea (Sinopharm Chemical Reagent Co., Ltd, Specpure) were dissolved in distilled water to make transparent solutions. In all cases, the concentration of Y^{3+} was kept at 0.015 M while urea was kept at 0.5 M. Doping levels of Nd^{3+} was kept at 2 at% the concentration of Y^{3+}. Ammonium sulfate $(NH_4)_2SO_4$ (Sinopharm Chemical Reagent Co., Ltd, Specpure) was added according to ratio $(NH_4)_2SO_4/Nd:Y_2O_3$ (theoretical yield) at various ratios from 0 wt% to 40 wt%. The mixed solution was homogenized and then heated to 90 °C within 1 h and then held for 2 h at 90 °C. Resultant precursors were collected *via* suction filtration. Byproducts of the reaction were removed by washing the particles with distilled water *via* suction filtration four times. After rinsing with anhydrous ethanol, the particles were dried in an air oven at 100 °C for 10 h and then calcined at 1100 °C for 4 h. The calcined powders were ground and sieved through 100 mesh screen. The powders were uniaxially pressed into pellets (ϕ 13 mm) under a pressure of 200 MPa. Then the pellets were sintered at 1730 °C for 4 h at the vacuum of 5.0×10^{-4} Pa in a furnace with a tantalum heating element (ZR-50-21, Shanghai, China).

To investigate the mechanism of the effect of ammonium sulfate on the preparation of the precursor, original transparent solutions with an ammonium sulfate ratio of 0 wt%, 10 wt%, 20 wt%, 30 wt%, 40 wt% were placed at 25 °C for 180 days so that an extreme slow growth of the corresponding precursor could be achieved.

Morphology of precursor prepared with different ammonium sulfate was observed by transmission electron microscopy (TEM, JEM-100CX, Japan) and field emission scanning electron microscope (SEM, S-4800, Japan). Fourier transform infrared spectroscopy (FTIR, NEXUS 670, USA) was performed to analyse the constitution evolution of the as prepared precursor. The zeta potential of the precursor suspended in deionized water was measured using a zeta potentiometer (Zetapals, Brookhaven Instruments Corporation, USA). Thermogravimetry (TG, Pyris Diamond, Perkin Elmer) of the dried precursor particles was made under flowing air (100 mL min^{-1}) with a heating rate of 10 °C min^{-1}. Phase identification was performed *via* X-ray diffractometry (XRD) on a X-ray diffractometer (Cu-Kα, Bruker model D8).

Results and discussion

The SEM micrographs of different precursors are shown in Fig. 1. Uniform spherical precursors with average diameters around 250 nm (see Fig. 1a) were obtained without ammonium sulfate as a control agent during synthesis. Aggregated particles with scale up to tens of microns were obtained with 10 wt% ammonium sulfate added (see Fig. 1b). Those embryo like particles are a result of the aggregation of sub-spheres ranging from 5–10 microns. Morphologies of the aggregations obtained at different ammonium sulfate dosage from 10 wt%–40 wt% are similar. However, these particles are actually composed of primary particles with specific morphology. Aggregated particles with rough surfaces composed of coadjacent grains with diameters about 80 nm were obtained when ammonium sulfate was added up to 10 wt% (see Fig. 1c). Coral like microstructures with tentacles about 20–30 nm in width, branch like microstructures with random structures as well as rod like surfaces with whiskers about 30 nm in width could be observed as the ammonium sulfate level reaches 20 wt%, 30 wt% and 40 wt%, respectively

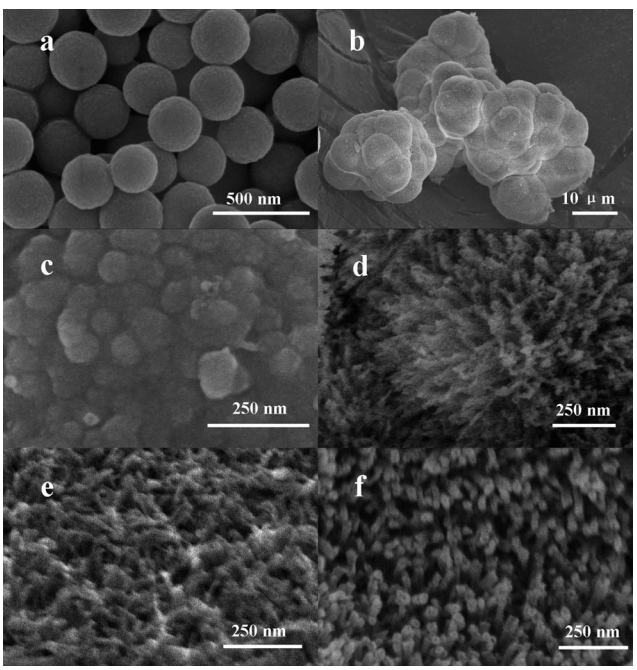

Fig. 1 SEM micrographs showing the precursors prepared with different dosages of $(NH_4)_2SO_4$. (a) Sample prepared with 0 wt% $(NH_4)_2SO_4$ added, (b) Sample prepared with 10 wt% $(NH_4)_2SO_4$ added, (c) Surface morphology of sample prepared with 10 wt% $(NH_4)_2SO_4$ added, (d) Surface morphology of sample prepared with 20 wt% $(NH_4)_2SO_4$ added, (e) Surface morphology of sample prepared with 30 wt % $(NH_4)_2SO_4$ added, (f) Surface morphology of sample prepared with 40 wt% $(NH_4)_2SO_4$ added.

This journal is © The Royal Society of Chemistry 2012

(see Fig. 1d, e, f). It is clear that the surface structure of the precursors can be adjusted in the presence of ammonium sulfate. The morphology shown in Fig. 1 could also be observed from the precipitation at an extremely slow rate (see Fig. 2) as a separate experiment.

Original transparent solutions with different dosages of ammonium sulfate were placed at 25 °C for 180 days so that an extreme slow growth of the corresponding precursor could be achieved. The decomposition constant of urea in water at 25 °C is calculated to be 6.65×10^{-8} s^{-1}, which is about 1/15 000 of the value of the decomposition constant of urea in water at 90 °C.[44] Flocculent sediment can be observed at the bottom of each solution. The resultant sediment was collected and then observed by transmission electron microscope. Fig. 2 shows the morphology of the particles. It can be seen from Fig. 2a that complete amorphous particles were formed without ammonium sulfate as a surfactant. Regular particles were gradually formed as ammonium sulfate was introduced into the solution. The amorphous floccules started to aggregate to be spongy particles when the ammonium sulfate was added up to 10 wt% (see Fig. 2b). Particles with clear appearance could be formed when the ammonium sulfate was added up to 20 wt% (see Fig. 2c). However, appearance of the aggregated grain like particles was still not quite regular when its scale reached 20–30 nm. Various particles with random structures could be observed in the precursor prepared with 30 wt% ammonium sulfate added. However, most of the particles are nanowires self-assembled from nanoparticles (see Fig. 2d). As the level of ammonium sulfate reaches 40 wt%, only regular nanowires 50–100 nm in width and 200–500 nm in length could be observed in the precursor. Coincidence between the morphology of these particles and the surface morphology of their corresponding precursor prepared at 90 °C (see Fig. 1) can be observed. Surface structures of those particles prepared at 90 °C were actually formed according to the particle structure shown in Fig. 2. These experimental results indicated that ammonium sulfate played an important role in the morphology control of Nd:Y_2O_3 precursors obtained by urea based homogeneous precipitation process.

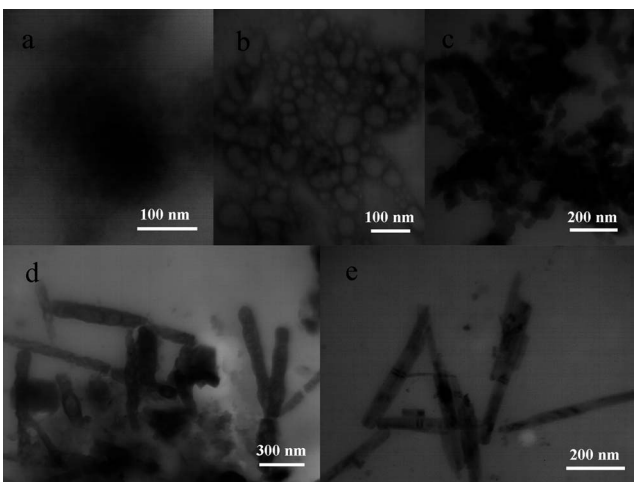

Fig. 2 Morphology of colloidal particles prepared at 25 °C with different dosages of $(NH_4)_2SO_4$. (a) 0 wt% (b) 10 wt% (c) 20 wt% (d) 30 wt % (e) 40 wt%.

The zeta potential of the Nd:Y_2O_3 precursors prepared with different dosages of ammonium sulfate at 90 °C is shown in Fig. 3. The positive zeta potential of the precursors is obviously decreased with the increase of ammonium sulfate. The decline of the zeta potential induces the synthesized precursors to aggregate and settle quickly in the solution. No obvious change in the zeta potential of the precursor particles is observed when the dosage of ammonium sulfate exceeds 20 wt%. The nose-dive of the zeta potential when ammonium sulfate is added below 10 wt% indicates the quick decline of potential in the stern layer of the particle. That could be attributed to the addition of sulfate ions. The sulfate ions possess more negative charges than OH^-, HCO_3^-, *etc.*, which can cause even obvious potential drop of the particle. However, the stabilization of zeta potential in the reaction system as the amount of ammonium sulfate exceeds 20 wt% indicates that the ion adsorption on the precursor surface becomes balanced. With further increases in the ammonium sulfate levels, the sulfate ions could not be adsorbed onto the surface of the precursor particles owing to the repulsive forces from the same kind of charges.

Fig. 4 shows the IR spectrum of the precursors with different dosages of ammonium sulfate added. It can be seen that with the increase of ammonium sulfate, there are obvious absorption peaks that emerged at 1115.8 cm^{-1} and 1446.3 cm^{-1} which could be indexed as the stretching vibrations of SO_4^{2-} and CO_3^{2-}, respectively. The FTIR spectra supply evidence for the absorption of SO_4^{2-}, which contributes to the significant drop of the zeta potential of the precursors shown in Fig. 3. As to the increasing absorption of CO_3^{2-}, a possible mechanism for the formation of Y_2CO_3 along with $Y(OH)CO_3$[2] is shown as follows:

At temperatures up to 83 °C, the aqueous solution of urea yields ammonium and cyanate ions.[40]

$$H_2NCONH_2 \rightleftharpoons NH_4^+ + OCN^- \quad (1)$$

In an acid solution, cyanate ions react rapidly according to

$$OCN^- + 2H^+ + H_2O \rightarrow CO_2 + NH_4^+ \quad (2)$$

Yttrium ions are hydrolyzed to $YOH(H_2O)_n^{2+}$ [41,42]

$$Y^{3+} + (n+1)H_2O \rightleftharpoons YOH(H_2O)_n^{2+} + H^+ \quad (3)$$

The precipitation of the basic carbonate could therefore be described by the following reaction:

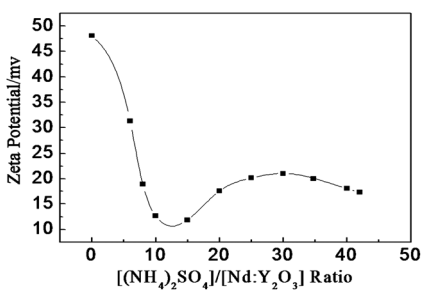

Fig. 3 Zeta potential of the Nd:Y_2O_3 precursor prepared with different dosages of $(NH_4)_2SO_4$.

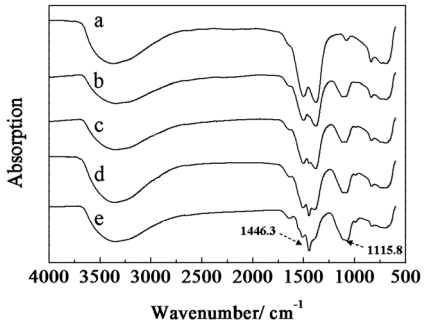

Fig. 4 Infrared spectrum of Nd:Y_2O_3 precursor prepared with different dosages of $(NH_4)_2SO_4$. (a) 0 wt% (b) 10 wt% (c) 20 wt% (d) 30 wt% (e) 40 wt%.

$$YOH(H_2O)_n^{2+} + H_2O + CO_2 \rightarrow Y(OH)CO_3 \cdot xH_2O + 2H^+ + (n - x)H_2O \quad (4)$$

When $(NH_4)_2SO_4$ exists in the precipitation system, NH_4^+ hydrolyzes, so that H^+ is released into the solution

$$NH_4^+ + H_2O \rightleftharpoons H_3 \cdot H_2O + H^+ \quad (5)$$

That resulting release of H^+ weaken the hydrolysis of the yttrium ions which accelerates urea decomposition. More CO_3^{2-} ions are released into the solution, which further contributes to the formation of Y_2CO_3.[25,41]

$$2Y(H_2O)_n^{3+} + 3H_2O + 3CO_2 \rightarrow Y_2(CO_3)_3 \cdot xH_2O + 6H^+ + (2n - x)H_2O \quad (6)$$

Fig. 5 exhibits the decomposition behaviour of the precursors measured by thermogravimetry, TG. Complete decomposition of the precursor prepared without ammonium sulfate occurs up to about 800 °C and the weight loss is 41.8 wt%. More weight loss happened from 900–1100 °C can be observed from the TG curve of the precursors prepared when ammonium sulfate was introduced into the precipitation system. Weight loss values of the precursors prepared with 10 wt%, 20 wt%, 30 wt% and 40 wt% ammonium sulfate added were 42.6 wt%, 47.9 wt%, 51.4 wt% and 52.1 wt%, respectively. That indicates the existence of SO_4^{2-} in the precursors, consistent with the result of the IR spectrum

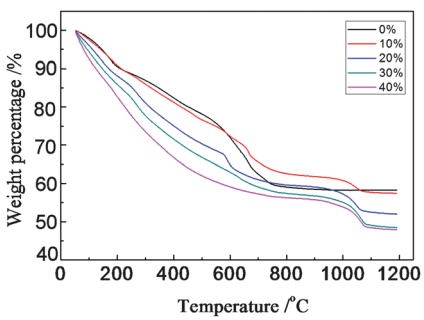

Fig. 5 Decomposition behavior of the dried particles prepared with different dosages of $(NH_4)_2SO_4$ added.

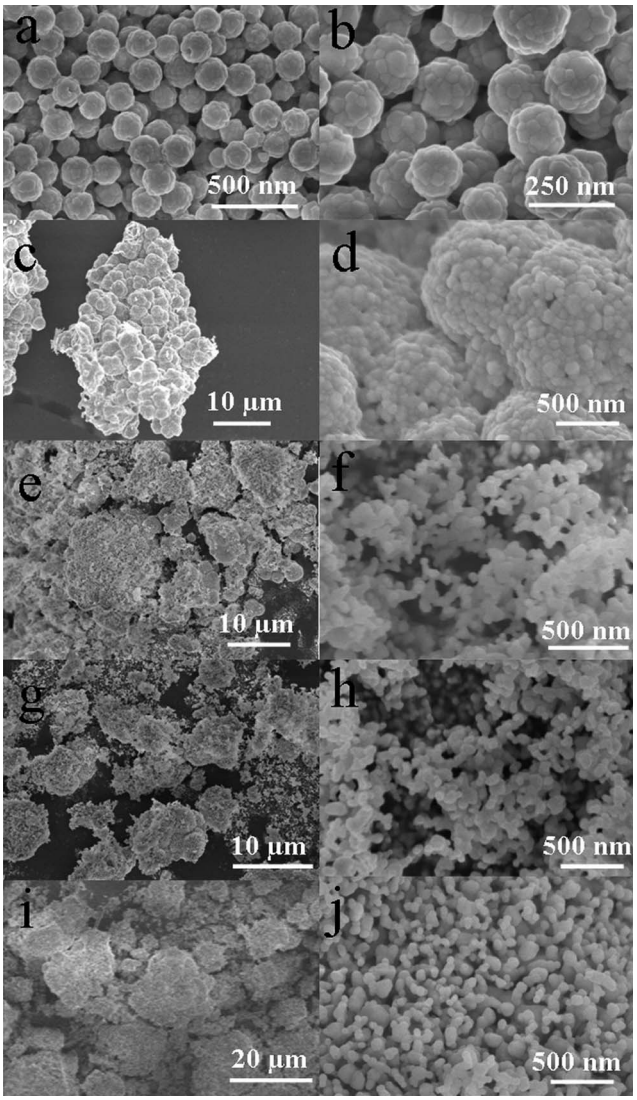

Fig. 6 SEM micrographs showing the 1100 °C calcined samples prepared with different dosages of $(NH_4)_2SO_4$. (a–b) Samples prepared with 0 wt% $(NH_4)_2SO_4$ added, (c–d) Samples prepared with 10 wt% $(NH_4)_2SO_4$ added, (e–f) Surface morphology of samples prepared with 20 wt% $(NH_4)_2SO_4$ added, (g–h) Surface morphology of samples prepared with 30 wt% $(NH_4)_2SO_4$ added, (i–j) Surface morphology of samples prepared with 40 wt% $(NH_4)_2SO_4$ added.

shown in Fig. 4. By measuring the weight loss values around 1000 °C, it is possible to estimate the weight percentage of SO_4^{2-} in the precursors. The weight loss values around 1000 °C of the precursors prepared with 0 wt%, 10 wt%, 20 wt%, 30 wt% and 40 wt% ammonium sulfate added were 0 wt%, 4.42 wt%, 6.97 wt%, 8.03 wt% and 8.04 wt%, respectively. No further weight loss is observed when the temperature is higher than 800 °C in the TG curve of the precursor prepared without ammonium sulfate. The weight loss value 8 wt% should be saturation absorption value of SO_4^{2-} into the precursors. That indicates that the absorption balance of SO_4^{2-} exists in the precipitation system, consistent with the result of the zeta potential shown in Fig. 3.

Micrographs of the 1100 °C calcined powders are shown in Fig. 6. Spherical particles with strong necking phenomena can be

This journal is © The Royal Society of Chemistry 2012

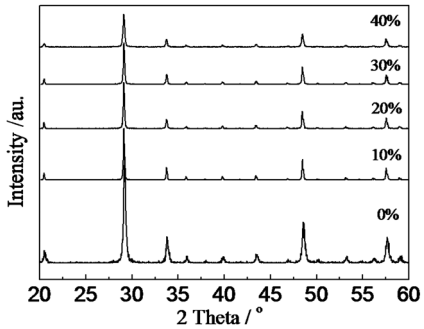

Fig. 7 XRD pattern at room temperature for the 1100 °C calcined samples prepared with different dosages of $(NH_4)_2SO_4$.

observed in Fig. 6a. Those particles with average sizes around 200 nm (see Fig. 6b) were the calcinate of the particles shown in Fig. 1a during whose preparation procedure ammonium sulfate was not added. Appearance of those embryo like aggregations shown in Fig. 1b was kept after the calcinations (see Fig. 6c). Coadjacent grains with diameter about 50–70 nm were observed on the surface of the calcinate of particles obtained when the ammonium sulfate was added up to 10 wt% (see Fig. 6d). Precursors prepared with more ammonium sulfate than 10 wt% broke down and were dispersed as nanosized powders after calcination.

Uniform particles with scale around 50 nm were obtained for the calcinate of the precursors prepared with 20 wt% and 30 wt% ammonium sulfate added (see Fig. 6e, f, g, h). That could be attributed to the decomposition of SO_4^{2-} around 1000 °C. The decomposition of SO_4^{2-} weakens the necking phenomenon during the calcinations of the precursors.[21] However, the particles obtained from the precursors prepared with 40 wt% ammonium sulfate are from collection of particles ranging from 50 nm–200 nm (see Fig. 6i, j). That could be attributed to the formation of the calcinate from different components that exist in the precursors. Different decomposition behaviors of $Y_2(CO_3)_2$ and $Y(OH)CO_3$ lead to a wider size distribution for the calcinate.

Fig. 7 shows the XRD pattern at room temperature for the 1100 °C calcined samples prepared with different dosages of ammonium sulfate. Pure Y_2O_3 could be prepared from all the precursors. However, the crystallinity of different calcinates exhibit obvious differences. The calcinate of precursors prepared with no ammonium sulfate exhibits the best crystallinity whilst when ammonium sulfate was introduced into the precipitation, the crystallinity of its corresponding calcinate declined along with the addition of ammonium sulfate. That could be attributed to the decomposition of SO_4^{2-} around 1000 °C (see Fig. 5).

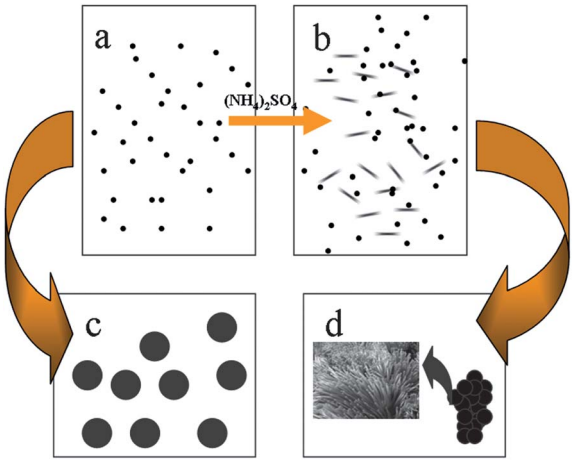

Fig. 9 Schematic demonstration and mechanism of the precipitation process. (a) Homogeneous nucleation without the addition of $(NH_4)_2SO_4$ (b) Different nucleation process with the addition of $(NH_4)_2SO_4$ (c) Homogeneous growth of colloidal particle without the addition of $(NH_4)_2SO_4$ (d) Aggregation process of the colloidal particle with the addition of $(NH_4)_2SO_4$.

Fig. 8 shows the picture of the sintered Nd:Y_2O_3 samples prepared from different nanopowders. According to the sintering experiment on the nanopowders, transparent ceramic yttria can be easily prepared with 20 wt% ammonium sulfate added. That indicates that the nanopowders exhibit the best sinterability when the softly aggregated particles were formed. With the addition of increasing amounts of ammonium sulfate (30 wt%, 40 wt%) into the precipitation system, the sinterability of the nanopowders gradually came down. That could be attributed to the decline of the uniformity of the particles (see Fig. 6j).

Based on the above experiments, the suggested precipitation mechanism is schematically shown in Fig. 9. When urea decomposed markedly at 83 °C, homogeneous nucleation happened so that sphere like precursors were prepared. With the addition of ammonium sulfate, constitution of the precursors, together with its zeta potential was changed. Two different nucleation process happened as the ammonium sulfate was added into the precipitation system. $Y_2(CO_3)_3$ also formed during the original nucleation process of $Y(OH)CO_3$. Nucleation processes were thereby changed. The sulfate ion absorbed into the stern layer of the colloidal particles declined the zeta potential of the particles and hereby caused the obvious aggregation of the colloidal particles. Weakly aggregated particles of large size were prepared (see Fig. 1b) rather than the uniform spherical particles (see Fig. 1a) grown in the homogeneous precipitation process. As ammonium sulfate was increased, its function as a structural

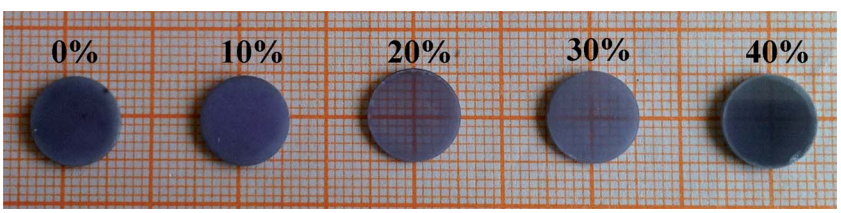

Fig. 8 Sintered Nd:Y_2O_3 samples prepared from precursors with different dosage of $(NH_4)_2SO_4$.

director mediating nanoparticle growth and assembly becomes clear. Coral like, branch like and rod like aggregated particles were prepared with different amounts of ammonium sulfate added. The absorption of SO_4^{2-} could induce anisotropic growth in an isotropic medium by adjusting the surface charge of the newly formed nucleus. Anisotropic absorption of SO_4^{2-} on different facets of the nucleus would regulate the growth of the nucleus. The facet with positive charges (Y^{3+}) would be more likely to absorb SO_4^{2-} to form a stereospecific blockade. These facets were thereby preserved, the anisotropic morphology of the seed formed in the earlier stage could lead to the formation of one dimensional nanostructures through non-symmetrical growth. In general, by adjusting the weight ratios of mediator to products ($(NH_4)_2SO_4$ to $Nd:Y_2O_3$) in the synthetic environment, the crystal growth pathway can be changed thermodynamically and kinetically at varying degrees. Thermodynamic control can be achieved by altering the surface energy and constitution of prepared materials, kinetic control can be achieved by altering the dosage of the mediator.[45–48]

Conclusions

$Nd:Y_2O_3$ precursors of different morphologies with uniform scale were achieved *via* a urea precipitation method. The effects of the amount of ammonium sulfate throughout the preparation process were intensively discussed. With the addition of ammonium sulfate, the constitution of the precursors, together with its zeta potential was changed. Both the nucleation and growth procedure of the precipitation process were adjusted. Coral like, branch like and rod like aggregated particles were prepared with different amounts of ammonium sulfate added. $Nd:Y_2O_3$ nanopowders prepared from those precursors exhibited entirely different sinterabilities. Nanopowders exhibited the best sinterability when the softly aggregated particles (see Fig. 1d) were formed. Results shown in this paper can contribute to the controllable synthesis of sinterable yttria nanopowders and further exploration of the mechanism of the precipitation process *via* a urea precipitation method.

Acknowledgements

This research was supported by the NSFC (Grant: 50990303, NSFDYS: 5092525, 050872070, 81102229, IRG: 50721002), and the Program of Introducing Talents of Discipline to Universities in China (111 program No. b06015), Independent Innovation Foundation of Shandong University (2010JQ004) and Shandong Provincial Natural Science Foundation, China (JQ201117).

Reference

1 R. A. Lefever and J. Matsko, *Mat. Res. Bull.*, 1967, **2**(9), 865–869.
2 Ji-Guang Li, Xiaodong Li, Xudong Sun, Takayasu Ikegami and Takamasa Ishigaki, *J. Chem. Mater.*, 2008, **20**, 2274–2281.
3 Ji-Guang Li, Xiaodong Li, Xudong Sun and Takamasa Ishigaki, *J. Phys. Chem. C*, 2008, **112**, 11707–11716.
4 R. C. Andersson, U.S. Patent 3545987 (1972).
5 J. Lu, T. Murai, T. Murai, K. Takaichi, T. Uematsu, K. Ueda, H. Yagi, T. Yanagitani and A. A. Kaminskii, *Jpn. J. Appl. Phys.*, 2001, **40**, 1277–1279.
6 Shirakawa, K. Takaichi, H. Yagi, J.-F. Bisson, J. Lu, M. Musha and K. Ueda, *Opt. Exp.*, 2003, **11**, 2911–2916.
7 J. Kong, D. Y. Tang, J. Lu, K. Ueda, H. Yagi and T. Yanagitani, *Opt. Lett.*, 2004, **29**, 1212–1214.
8 B. M. Walsh, J. McMahon, W. C. Edwards, N. Barnes, R. W. Equall and R. L. Hutcheson, *J. Opt. Soc. Am. B*, 2002, **19**, 2893–2903.
9 G. C. Wei, C. Brecher, M. R. Pascucci, E. R. Trickett and W. H. Rhodes, *SPIE Proc.*, 1988, **929**, 50–56.
10 P. H. Kleinand and W. J. Croft, *J. Appl. Phys.*, 1967, **38**, 1603–1607.
11 O. N. Carlsson, *Bull. Alloy Phase Diagrams*, 1990, **11**(1), 61–66.
12 Philippe Veber, Matias Velázquez, Véronique Jubera, Stanislav Péchev and Oudomsack Viraphong, *CrystEngComm.*, 2011, **13**, 5220–5225.
13 T. Yanagitani, H. Yagi, and M. Ichikawa, Japanese Patent 10–10133 (1998).
14 J. Lu, K. Ueda, H. Yagi, T. Yanagitani, Y. Akiyama and A. A. Kaminskii, *J. Alloy Compd.*, 2002, **341**, 220–225.
15 Jian Zhang, Liqiong An, Min Liu, Shunzo Shimai and Shiwei Wang, *J. Eur. Ceram. Soc.*, 2009, **29**, 305–309.
16 Karn Serivalsatit, Baris Kokuoz, Basak Yazgan-Kokuoz, Marian Kennedy and John Ballato, *J. Am. Ceram. Soc.*, 2010, **93**(5), 1320–1325.
17 L. R. Furlong and L. P. Domingues, *Ceram. Bull.*, 1966, **45**(12), 1051–1054.
18 M. D. Rasmussen, G. W. Jordan, M. Akinc, O. Hunter, Jr. and M. F. Berard, *Ceram. Int.*, 1983, **9**, 59–60.
19 R. Subramanian, P. Shankar, S. Kavithaa, S. S. Ramakrishnan, P. C. Angelo and H. Venkataraman, *Mater. Let.*, 2001, **48**, 342–346.
20 M. D. Fokema, E. Chiu and J. Y. Ying, *Langmuir*, 2000, **16**, 3154–3159.
21 T. Ikegami, J. G. Li, T. Mori and Y. Moriyoshi, *J. Am. Ceram. Soc*, 2002, **85**(7), 1725–1729.
22 N. Saito, S. Matsuda and T. Ikegami, *J. Am. Ceram. Soc.*, 1998, **81**(8), 2023–2028.
23 D. Sordelet and M. Akinc, *J. Colloid Interface Sci.*, 1988, **122**, 47–59.
24 M. Ciftcioglu, M. Akinc and L. Burkhart, *J. Am. Ceram. Soc.*, 1987, **70**(11), 329–334.
25 Bar Aiken, Wan Peter HSU and Egon Matijević, *J. Am. Ceam. Soc.*, 1988, **71**(10), 845–853.
26 H. Tomaszewski, H. Weglarz and R. De Gryse, *J. Eur. Ceram. Soc.*, 1997, **17**, 403–406.
27 P. K. Sharma, M. H. Jilavi, R. Naß and H. Schmidt, *J. Mat. Sc. Lett.*, 1998, **17**, 823–825.
28 Xing Zhang, Peng Hu, Yue-Bin Cao, Wei-Cheng Xiang, Ming-Shui Yao, Hai-Bao Zhang, Fang-Li Yuan and Rui-Fen Xu, *CrystEngComm.*, 2011, **13**, 3057–3063.
29 Yuhua Zheng, Hongpeng You, Guang Jia, Kai Liu, Yanhua Song, Mei Yang, Yeju Huang and Hongjie Zhang, *CrystEngComm.*, 2010, **12**, 585–590.
30 M. Akinc and A. Celikkaya, *Adv. Ceram.*, 1987, **21**, 57–67.
31 T. Hours, P. Bergez, J. Charpoin, A. Larbot, C. Guizard and L. Cot, *Am. Ceram. Soc. Bull.*, 1992, **71**, 200–203.
32 A. J. Rulison and R. C. Flagan, *J. Am. Ceram. Soc.*, 1994, **77**, 3244–3250.
33 A. L. Micheli, *Ceramic Powder Science II*, 1988, **1**, 102–109.
34 Y. Minagawa and F. Yajima, *Bull. Chem. Soc. Jpn.*, 1990, **63**, 378–382.
35 C. Greskovich, C. R. O'Clair and M. J. Curran, *J. Am. Ceram. Soc.*, 1972, **55**(6), 324–328.
36 B. Djuricic, D. Kolar and Mustafa Memic, *J. Eur. Ceram. Soc.*, 1992, **9**, 75–82.
37 A. Dupont, C. Parent, B. Le Garrec and J. M. Heintz, *J. Solid State Chem.*, 2003, **171**, 152–160.
38 S. Ekambaram and K. C. Patil, *J. Mater. Chem.*, 1995, **5**, 905–908.
39 N. Dasgupta, R. Krishnamoorthy and T. Jacob, *Int. J. Inorg. Mater.*, 2001, **3**, 143–149.
40 T. Sugimoto, *Adv. Colloid Interface Sci.*, 1987, **28**, 65–108.
41 D. E. Ryabchikov, and V. A. Ryabukhin, Ann Arbor MI.1970, 50–60.
42 C. F. Base, and R. E. Mesmer, *The hydrolysis of Cations*. Wiley, Newyork. 1976, 129–146.
43 Yu. L. Kopylov, V. B. Kravchenko, A. A. Komarov, Z. M. Lebedeva and V. V. Shemet, *Opt. Mater.*, 2007, **29**, 1236–1239.
44 W. H. R. Shaw and John J. Bordeaux, *J. Am. Chem. Soc.*, 1955, **77**, 4729–4733.

 This journal is © The Royal Society of Chemistry 2012

45 J. Chen, T. Herricks, M. Geissler and Y. Xia, *J. Am. Chem. Soc.*, 2004, **126**, 10854–10855.
46 H. Song, F. Kim, S. Connor, G. A. Somorjai and P. Yang, *J. Phys. Chem. B*, 2005, **109**, 188–193.
47 V. F. Puntes, K. M. Krishnan and P. Alivisatos, *Appl. Phys. Lett.*, 2001, **78**, 2187–2189.
48 V. F. Puntes, K. M. Krishnan and A. P. Alivisatos, *Science*, 2001, **291**, 2115–2117.